Available online at www.sciencedirect.com
SCIENCE DIRECT®
Organic Electronics 5 (2004) 257–263
Organic Electronics
www.elsevier.com/locate/orgel

Early stages of pentacene film growth on silicon oxide

Alex C. Mayer [a], Ricardo Ruiz [a], Randall L. Headrick [b], Alexander Kazimirov [c], George G. Malliaras [a,*]

[a] *Materials Science and Engineering, Cornell University, Ithaca, NY 14853 1501, USA*
[b] *Department of Physics, University of Vermont, Burlington, VT 05405, USA*
[c] *Cornell High Energy Synchrotron Source, Ithaca, NY 14853, USA*

Received 27 January 2004; accepted 7 May 2004
Available online 15 June 2004

Abstract

Among the various materials suitable for organic thin-film transistors (OTFTs), pentacene stands out as a model molecule, exhibiting one of the highest field effect mobilities reported so far. Understanding the growth mechanism of pentacene on dielectrics is essential for controlling film morphology and for fabricating high quality, large-grain, defect-free films. Such films will help us gain insight into the fundamentals of transport in organic films as well as enable the ultimate OTFT performance. In situ synchrotron X-ray scattering was used to probe the early stages of pentacene growth on SiO_2 in real time and under conditions relevant to the fabrication of OTFTs. Reflectivity measurements reveal that a thin layer of water, initially present on the substrate, is trapped at the interface when the pentacene film is deposited. Therefore, the interface relevant for OTFTs is that between pentacene and water. Anti-Bragg oscillations, observed for the first time during organic film growth, reveal that the first monolayer of pentacene completes fully before the second one nucleates. Subsequent layers nucleate before the underlying layers complete, giving rise to the characteristic island structure observed in pentacene films used in OTFTs. A simple distributed growth model was found to adequately describe the growth mechanism.

1. Introduction

The strong tendency of pentacene to form polycrystalline films has made it an attractive molecule for applications in organic thin-film transistors (OTFTs) [1]. Pentacene OTFTs with p-channel field effect mobilities exceeding 1 $cm^2/V\,s$ have been fabricated [2,3]. Hybrid complementary MOS circuits, using a-Si:H as the n-channel transistors have been demonstrated, indicative of the potential of organics to complement silicon [4]. Charge transport in OTFTs is believed to take place at the first monolayer near the interface with the gate dielectric [5] (typically SiO_2), with the quality of the organic/dielectric interface playing a critical role in determining the field effect mobility. This has motivated several studies of organic semiconductor growth on SiO_2, as well as other substrates [6–13].

Synchrotron X-ray sources offer unique advantages for studying early stages of film

* Corresponding author. Tel.: +1-607-2551956; fax: +1-607-255-2365.
E-mail address: george@ccmr.cornell.edu (G.G. Malliaras).

1566-1199/$ - see front matter © 2004 Elsevier B.V. All rights reserved.
doi:10.1016/j.orgel.2004.05.001

growth. The high intensity and excellent collimation of synchrotron X-ray beams enables studies of films down to the submonolayer regime. Synchrotron radiation was recently utilized to quantify the degree of ordering in pentacene films deposited on anisotropic substrates [14], and has also been applied to monitor the formation of the first pentacene layers on oxidized and hydrogen terminated silicon substrates [13]. Synchrotron X-ray studies on pentacene films also include diffuse scattering of submonolayer films in the aggregation regime to verify the diffusion-limited process of film formation [12].

In the present work we use synchrotron X-ray scattering to monitor pentacene growth on SiO_2. The experimental conditions were chosen for their high relevance to the fabrication of OTFTs. Namely, SiO_2 (the most commonly utilized gate dielectric in OTFTs reported to date [1]) was used as the substrate and was held at room temperature during the deposition. Film growth took place under high vacuum, in agreement with the vast majority of the work on OTFT fabrication. We confirm that, under such conditions, a thin layer of water is present on the SiO_2. Pentacene is found to grow on top of the water layer by fully completing the first monolayer before nucleating the second one. Subsequent layers nucleate before the layers underneath complete, giving rise to the rough topography observed in films used in OTFTs. A simple distributed growth model was found to adequately describe pentacene growth.

2. Experimental

Pentacene films were prepared in a custom made vacuum evaporator (Advanced Design Consulting, Inc.), which was mounted in a four circle diffractometer at the A2 station of the Cornell High Energy Synchrotron Source (CHESS). Substrates consisted of [1 0 0] p-type silicon wafers with a 3000 Å thermal oxide grown at the Cornell Nanofabrication Facility. The substrates were cleaned prior to deposition in an ultrasonic bath with deionized water, dried with filtered, dried nitrogen, and given a UV/ozone treatment. Pentacene films were deposited in high vacuum (10^{-6} Torr) onto substrates held at room temperature. A two-chamber boat (R.D. Mathis SO-20) was used as the source, and the rate of deposition was approximately 0.44 ML/min, as measured by a quartz crystal microbalance (QCM). The QCM was calibrated using X-ray reflectivity measurements as well as AFM measurements in sub-ML thick films. Film growth was monitored during deposition at CHESS by using 10.05 keV X-rays with a flux of $\sim 10^{13}$ photons/s, incident to the sample through a Be window. Both θ–2θ scans, as well as intensity measurements in the anti-Bragg configuration as a function of time were taken during growth. A scintillator counter was used for measuring the scattered X-ray intensity. After deposition, atomic force microscopy was conducted ex situ in tapping mode using a DI 3100 Dimension microscope.

3. Results and discussion

The surface structure of oxides depends on the reactions of dangling bonds [15]. In silicate glasses, such as SiO_2, formation of surface leads to Si–O- and Si-bonds that are unsaturated. These bonds react rapidly with atmospheric water to form Si–OH groups [15]. Therefore, the surface of SiO_2 is normally composed of hydroxyl groups. Once hydroxylated, the SiO_2 surface will attract water and become covered with a thin layer of water. Although the presence of water on SiO_2 surfaces is rather well documented [15, and references within], there is little systematic information about the thickness of the water layer. This is partly due to the fact that small amounts of water (a few monolayers) are hard to detect using common analytical techniques, and party due to the fact that the thickness of the water layer depends on the oxide fabrication process, the storage conditions as well as the cleaning procedures used [16].

Condensation of water on SiO_2 will also take place under high vacuum, since at 10^{-6} mbar the typical monolayer formation time is of the order of a second. Indeed, synchrotron X-ray reflectivity measurements from SiO_2 surfaces kept in high vacuum and at room temperature revealed the presence of a water layer with thickness of 7 Å (on thermal SiO_2 [13]), and of 6.5 Å (on SiO_2 made by

the Shiraki method [16]). The specular reflection of synchrotron X-rays from a SiO_2 substrate prepared as described in the experimental part is shown in Fig. 1(a). The data shows the expected decrease till approx. $q_z = 0.27$ Å^{-1}, where a broad feature, associated with the presence of a water layer [13,16], appears. As expected, the intensity of the feature diminished when the substrate was heated above room temperature, but promptly recovered when the substrate was allowed to cool back down to room temperature. The line in Fig. 1(a) is a fit to the data using a slab of charge with the density of water on top of the substrate, and reveals a thickness of 12 Å for the water layer on this particular case. The thickness of the water layer was found to depend on the exact preparation and cleaning of the substrate, but some water was always found to be present on the substrate at room temperature. However, when the SiO_2 was coated with hexadecyltrichlorosilane (a hydrophobic self-assembled monolayer), no water layer was found to condense on it, in agreement with studies of hydrophobic (hydrogenated) SiO_2 surfaces [16].

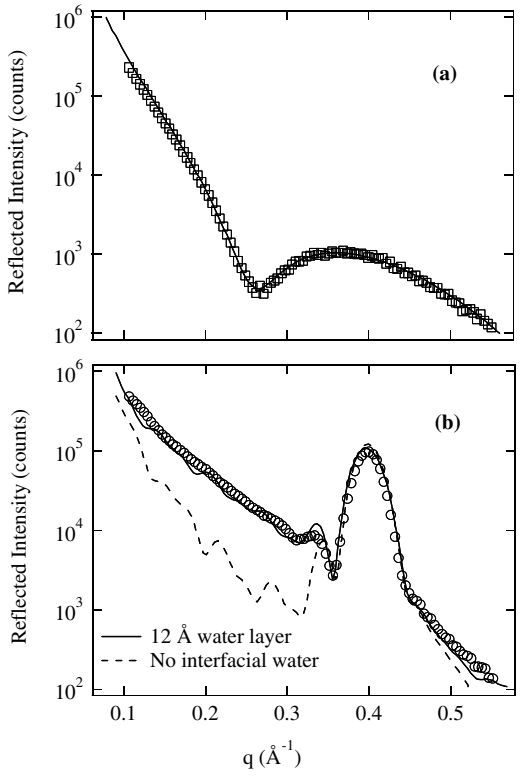

Fig. 1. θ–2θ scans from the substrate before (a) and after (b) deposition of 8.1 ML of pentacene. The solid lines are fits including a 12 Å thick layer of water on the SiO_2 substrate. The dashed line represents the expected intensity in the absence of the water layer.

The role of this water layer on the growth of organic semiconductor films has not received any attention. Namely, it is not known whether the water layer is displaced by the organic molecules (which are typically hydrophobic), or is trapped at the interface. The open circles in Fig. 1(b) show the specular reflection from a 8.1 monolayers (MLs) of pentacene deposited on the substrate discussed in the previous paragraph. Assuming that pentacene displaces the water layer leads to an underestimate of the reflectivity: The dashed line in Fig. 1(b) is a fit to the data for a 8.1 ML pentacene film on pristine SiO_2. On the other hand, the solid line in Fig. 1(b) is a fit to a model that includes the 12 Å thick water layer between the SiO_2 and the pentacene film. Clearly, the water layer that was originally present on SiO_2 is trapped at the interface when pentacene is deposited. This finding has major implications for the fabrication of OTFTs, as the interface of relevance is not that between pentacene and SiO_2, but rather the one between pentacene and water. Apart from having a different dielectric constant than SiO_2, the water layer might be responsible for charge trapping or even doping of the pentacene film. In addition, it might cause delamination of the pentacene film upon heating. The presence of a water layer might account for the large scatter of electrical data found in OTFT literature [1].

Pentacene grows on top of the water layer in the so-called thin-film phase [17]. The reflectivity curve from the pentacene film (Fig. 1(b)) shows the (0 0 1) Bragg reflection at $q_z = 0.3999$ Å^{-1}, which corresponds to an average layer spacing of 15.6 Å. This is substantially different than the layer spacing in pentacene crystals (14.5 Å [18]), but close to the 15.4 Å reported for the thin-film phase [17]—the small difference is probably caused by the error introduced due to the high background level at (0 0 1). Since the same thin-film phase has been observed in films grown on a variety of substrates [17,19,20] and under a variety of conditions, including ultra-high vacuum [21], it is unlikely that

water plays a major role in determining the structure of the pentacene film. The same evidence suggest that it is also unlikely that water is incorporated in the pentacene film. A determination of the structure of thin pentacene films is currently underway by means of in-plane scattering, and will be reported in a separate paper.

The question arises as to whether pentacene growth can be adequately described by a simple model. A powerful technique for monitoring thin-film growth is anti-Bragg scattering. In the kinematical approximation [22], the X-ray intensity for specular reflection by a thin film is given by

$$I = \left| r_{\text{sub}} e^{-i\phi} + r_{\text{film}} \sum_n \theta_n e^{-iqdn} \right|^2 \quad (1)$$

where r_{sub} is the reflection amplitude of the substrate, r_{film} is the amplitude from a layer of the film, θ_n is the coverage of the nth layer of the film, q is the momentum transfer, d is the layer spacing in the film, and ϕ is the phase difference between the waves reflected by the substrate and the first layer of the film. In the anti-Bragg configuration, q is chosen such that $q \cdot d = \pi$, which corresponds to the $(0\,0\,\frac{1}{2})$ reflection. In this configuration, the scattered intensity from a pentacene layer will cancel the intensity from the layer directly below. The destructive interference leads to increased sensitivity and has been used in the study of inorganic films such as growth of GaN films [23] and sputtering of Co films [24].

In Fig. 3(a), the intensity of the anti-Bragg reflection ($q_z = 0.19995$ Å^{-1}) during pentacene growth is plotted as a function of the total film thickness as measured with a quartz crystal microbalance. Anti-Bragg oscillations, where the local extrema correspond to integer number of layers, are clearly visible. The damping in the intensity of the oscillation as well as the fact that successive extrema are slightly shifted to higher thickness indicate that the film is getting rougher as it grows thicker.

A simple distributed growth model [25] was used to fit the data and extract the coverage of each layer, θ_n, as a function of time. In this model, molecules arrive at the film at an effective deposition rate v_{eff} (which accounts for possible desorption) and incorporate onto it. Molecules that land on top of the nth layer (where the 0th layer is the bare substrate) may diffuse and incorporate on the step edge of the $n+1$ layer, or transfer down to the top of the $n-1$ layer to be incorporated into the nth layer (see Fig. 2). Thermal desorption of molecules as well as transfer to the $n+1$ layer are neglected. The former is a good assumption for a substrate held at room temperature, while the latter is usually the case due to the asymmetry in the Erlich–Schwoebel barrier [26]. Accordingly, the rate of change for the coverage, θ_n, of the nth layer is then given by [25]

$$\frac{d\theta_n}{dt} = v_{\text{eff}}(\theta_{n-1} - \theta_n) - \alpha_{n-1} v_{\text{eff}}(\theta_{n-1} - \theta_n) + \alpha_n v_{\text{eff}}(\theta_n - \theta_{n+1}) \quad (2)$$

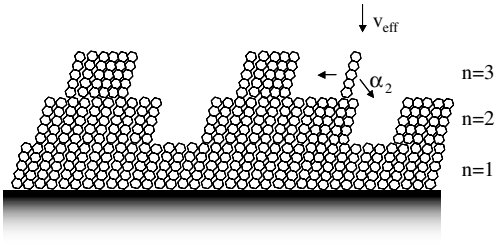

Fig. 2. Depiction of the elementary processes included in the model for pentacene film growth.

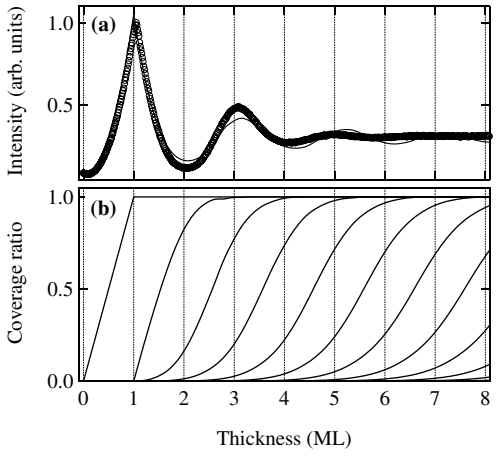

Fig. 3. (a) Anti-Bragg oscillations during pentacene growth. The line is a fit to the distributed model. (b) Calculated layer coverage vs. total coverage.

Eq. (2) states that of the $v_{\text{eff}}(\theta_{n-1} - \theta_n)$ adsorbates landing on top of the $n-1$ layer per unit time, a fraction α_{n-1} transfers down to the $n-1$ layer while a fraction $(1-\alpha_{n-1})$ remains on top of the $n-1$ layer to be incorporated into the step edges of the nth layer. Similarly, the third term in Eq. (2) accounts for the fraction α_n that transfers down from layer $n+1$ to the nth layer.

The parameters α_n in Eq. (2) measure the rate at which molecules transfer from the $n+1$ to the nth layer. Assuming that incoming adsorbates distribute according to the available number of energetically favorable sites such as steps or cluster edges, then α_n can be expressed in terms of the lateral cross section, d_n, of the nth layer. According to Cohen et al. [25] α_n is given by

$$\alpha_n = A_n \frac{d_n}{d_n + d_{n+1}} \tag{3}$$

where A_n accounts for the probability of a molecule sitting on the perimeter of the nth layer to jump down and join the nth layer. The limits of the model are perfect layer-by-layer growth for $A_n = 1$ and non-diffusive growth for $A_n = 0$ [25].

The lateral cross section of a layer, d_n, can be expressed as a function of the layer coverage. If s represents the area of a two-dimensional island and D its fractal (Hausdorff) dimension, then the island cross section is proportional to s^{p_1} [27,28], where $p_1 = 1/D$. For a compact island, $D = 2$; but for diffusion-limited aggregates, $D = 5/3$ [29,30]. Assuming that before percolation the island density, N, remains constant and composed of identical islands [12,28], then the total cross section of a layer becomes $d_n = Ns^{p_1}$ and since $\theta = Ns$, then $d_n \propto \theta^{p_1}$. Similarly, if after percolation the number of holes in the film also remains constant, then the linear cross section of each layer can be related to its coverage by [25]

$$d_n \propto \begin{cases} \theta_n^{p_1}, & \theta_n \leqslant \theta_c \\ (1-\theta_n)^{p_2}, & \theta_n \geqslant \theta_c \end{cases} \tag{4}$$

The two exponents are interrelated by $\theta_c^{p_1} = (1-\theta_c)^{p_2}$ [25], where θ_c indicates the coverage at which percolation occurs.

In the present work we have allowed A_n to be different at the layer in direct contact to the substrate $(A_1 = A_{\text{sub}})$ than in the rest of the film $(A_{n>1} = A_{\text{pent}})$ to account for a difference in the affinity of pentacene molecules for the substrate and for pentacene. The intensity in Fig. 3(a) shows a sharp cusp when the first monolayer is completed. This is due to the fact that the adsorbed material discretely shifts from adding to the first layer to adding to the second, indicating that the first monolayer on the substrate completes fully before the second monolayer begins to nucleate. Therefore, $A_{\text{sub}} = 1$ (the value for layer-by-layer). This is in agreement with AFM micrographs of single layer pentacene films grown on SiO_2 [13]. Moreover, it has been shown that pentacene islands develop a fractal shape during growth on SiO_2 [10,13] that resembles that of diffusion-limited aggregation, in which case $D = 5/3$, hence $p_1 = 0.6$. This reduces the number of independent parameters to four: A_{pent}, $r_{\text{sub}}/r_{\text{pent}}$, ϕ, and θ_c. This number was further reduced by using the first peak in Fig. 3(a) (where $\theta_1 = 1$ and $\theta_2 = 0$) to extract the ratio $r_{\text{sub}}/r_{\text{pent}}$, which was found to be equal to 0.305. The fact that $r_{\text{sub}}/r_{\text{pent}} < 1$ should not be regarded as a direct measurement of the density ratio between the substrate and pentacene because r_{sub} contains the reflection amplitude of the silicon wafer plus the oxide layer plus the water layer, as well as phase differences at the corresponding interfaces.

The solid line in Fig. 3(a) is the result of a fit of the parameters in Eqs. (1) and (2) with the X-ray data revealing $A_{\text{pent}} = 0.9$, $\theta_c = 0.54$, and $\phi = 1.4$ rad. The simple distributed model reproduces the essential features of the data and gives an adequate description of the pentacene growth process. The fact that $A_{\text{pent}} < A_{\text{sub}}$ is in agreement with the fact that the first layer completes fully before the second one begins to nucleate, while subsequent layers begin to nucleate before the layer underneath has completed. This is also shown in Fig. 3(b), which displays the fractional coverage for each layer as extracted from the solutions of the various θ_n. Finally, the coverage $\theta_c = 0.54$ at which coalescence occurs agrees with previous observations for pentacene on SiO_2 [13] for which $0.5 < \theta_c < 0.6$.

A comment is in order regarding the nature of the anti-Bragg oscillations. One possible source of the periodic variation in scattering intensity is

from an oscillation in the roughness of the surface as each monolayer nucleates and coalesces. This effect leads to a peak in the anti-Bragg intensity at integer monolayer coverages. But oscillations could also be due to thin-film interference effects (Kiessig fringes) [31]. The Kiessig fringes are expected produce anti-Bragg oscillations with a period of two monolayers rather than one, as we have observed in our pentacene growth experiments (Fig. 3(a)). The existence of oscillations from both effects are highly sensitive to surface roughness and islanding phenomena. Furthermore, both effects are accounted for in the simulations of the data shown in Fig. 3(a). However, in order to determine the origin of the oscillations, a separate experiment was performed where the intensity of both the specular and diffuse signals were measured during film growth (the latter was measured at $q_x = -5.3514 \times 10^{-4}$ Å^{-1}). The diffuse scattering, which is proportional to the structure factor of the film, also yields information about correlated and uncorrelated roughness. The diffuse intensity, for instance, is expected to develop a maximum corresponding to the lateral correlation length, i.e., the average inter-island distance. This maximum increases in intensity as the islands grow in size, reaches a maximum at $\theta_n = \theta_c$, and then vanishes every time the islands coalesce and form a full layer [12,28]. It was found that the diffuse signal (not shown here) exhibits maxima near 0.5 and 1.5 monolayers and minima near 1 and 2 monolayers. This is exactly the characteristic of roughness oscillations, which will also contribute to the specular signal, and therefore affect the shape of the curve in Fig. 3(a). Therefore, we conclude from these additional measurements that the overall periodicity of the anti-Bragg oscillations is related to the Kiessig effect, however the detailed shape of the data is determined by a combination of the Kiessig effect and a periodic oscillation in surface roughness.

In order to test the predictive power of the model, results were compared to AFM measurements of surface topography. The inset in Fig. 4 displays a characteristic AFM micrograph from a 3.35 ML thick pentacene film. A typical way to describe such data is to display a histogram of the percentage of each layer that is exposed. The open

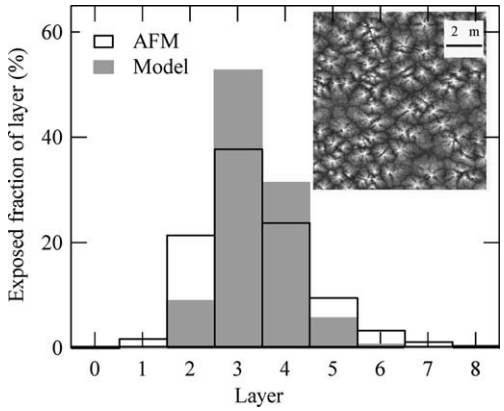

Fig. 4. Histogram showing the percentage of each layer that is exposed as calculated from an AFM micrograph (open bars), and as predicted by the model (gray bars). Inset: AFM micrograph of a 3.35 ML pentacene film.

bars in Fig. 4 display the histogram calculated from the AFM image on the inset. The largest fraction of exposed area corresponds to the third monolayer, while the first monolayer is completely covered, and the eighth one has not nucleated yet. The shaded bars in Fig. 4 display the same information calculated from the growth model according to the parameters obtained from the fit to anti-Bragg oscillations. The model successfully predicts that the third monolayer is the most exposed one and gives an adequate description of the overall film morphology. It yields, however, a histogram with a narrower distribution that is skewed towards higher coverage. This is because the deviation from a layer-by-layer growth gets more pronounced with increasing coverage as can be seen in Fig. 3(a), where the intensity oscillations basically disappear after the sixth layer. A more complex model, utilizing different A_n's for each layer, can capture these features better.

4. Conclusions

In conclusion, the growth of pentacene films on SiO_2 was investigated in situ and *in real time* by means of synchrotron X-ray scattering. Under high vacuum conditions, a layer of water was found to cover the SiO_2 substrate. Pentacene grew

on top of the water layer by fully completing the first monolayer before nucleating the second one. Subsequent layers nucleated before the layers underneath completed, giving rise to the rough topography observed in films used in OTFTs. The coverage at which pentacene islands coalescence was found to be equal to 0.54. Comparison with AFM measurements confirmed the validity of a simple distributed growth model that can be used to predict pentacene film morphology.

Acknowledgements

The authors are grateful to Jesse Salem (IBM Almaden), Santha Ambily and John Sinnott for help with the experiments and to James Engstrom, Dieter Ast, Michael Thompson, Rüediger Dieckmann, and all members of the IRG-D of the Cornell Center for Materials Research (CCMR) for fruitful discussions and valuable suggestions. This work was supported with grants from the CCMR, a Materials Research Science and Engineering Center of the National Science Foundation (DMR-9632275), from the Naval Research Laboratory (N00173-00-1-G003), and from the Department of Energy (DEFG0203ER46032). A portion of this work was conducted at the Cornell High Energy Synchrotron Source (CHESS), which is supported by the National Science Foundation under award DMR 97-13424, and at the Cornell Nanofabrication Facility (a member of the National Nanofabrication Users Network) which is supported by the National Science Foundation under Grant ECS-9731293.

References

[1] C.D. Dimitrakopoulos, P.R.L. Malenfant, Advanced Materials 14 (2002) 99–117.
[2] Y.Y. Lin, D.J. Gundlach, S.F. Nelson, T.N. Jackson, IEEE Electron Device Letters 18 (1997) 606–608.
[3] M. Halik et al., Journal of Applied Physics 93 (2003) 2977–2981.
[4] M. Bonse, D.B. Thomasson, H. Klauk, D.J. Gundlach, T.N. Jackson, IEDM Technical Digest 249 (1998).
[5] A. Dodabalapur, L. Torsi, H.E. Katz, Science, New Series 268 (1995) 270–271.
[6] S.R. Forrest, P.E. Burrows, E.I. Haskal, F.F. So, Physical Review B (Condensed Matter) 49 (1994) 11309–11321.
[7] F. Biscarini, R. Zamboni, P. Samon, P. Ostoja, C. Taliani, Physical Review B (Condensed Matter) 52 (1995) 14868–14877.
[8] P. Fenter, F. Schreiber, L. Zhou, P. Eisenberger, S.R. Forrest, Physical Review B (Condensed Matter) 56 (1997) 3046–3053.
[9] M. Brinkmann, F. Biscarini, C. Taliani, I. Aiello, M. Ghedini, Physical Review B (Condensed Matter) 61 (2000) R16339–16342.
[10] F.J. Meyer zu Heringdorf, M.C. Reuter, R.M. Tromp, Nature 412 (2001) 517–520.
[11] A.C. Durr et al., Physical Review Letters 90 (2003) 016104/1-4.
[12] R. Ruiz et al., Physical Review Letters 91 (2003) 136102/1-4.
[13] R. Ruiz et al., Physical Review B (Condensed Matter and Materials Physics) 67 (2003) 125406-1-7.
[14] M.L. Swiggers et al., Applied Physics Letters 79 (2001) 1300–1302.
[15] R.H. Doremus, Glass Science, John Wiley and Sons Inc., New York, 1994, Chapter 11.
[16] K. Shin, X. Hu, X. Zheng, M.H. Rafailovich, J. Sokolov, V. Zaitsev, S.A. Schartz, Macromolecules 34 (2001) 4993.
[17] C.D. Dimitrakopoulos, A.R. Brown, A. Pomp, Journal of Applied Physics 80 (1996) 2501–2508.
[18] R.B. Campbell, J.M. Robertson, J. Trotter, Acta Crystallographica 14 (1961) 705–711.
[19] M. Shtein, J. Mapel, J.B. Benziger, S.R. Forrest, Applied Physics Letters 81 (2002) 268–270.
[20] D. Knipp, R.A. Street, A. Volkel, J. Ho, Journal of Applied Physics 93 (2003) 347–355.
[21] R. Ruiz et al., in: S.C. Moss (Ed.), Organic Optoelectronic Materials, Processing and Devices. Symposium, Materials Research Society Symposium Proceedings, vol. 708, Materials Research Society, Warrendale, PA, 2002, pp. 415–421.
[22] B.E. Warren, X-Ray Diffraction, Addison-Wesley, Reading, Mass, 1969.
[23] A.R. Woll, R.L. Headrick, S. Kycia, J.D. Brock, Physical Review Letters 83 (1999) 4349–4352.
[24] O. Malis, J.D. Brock, R.L. Headrick, M.-S. Yi, J.M. Pomeroy, Physical Review B (Condensed Matter and Materials Physics) 66 (2002) 035408/1-9.
[25] P.I. Cohen, G.S. Petrich, P.R. Pukite, G.J. Whaley, A.S. Arrott, Surface Science 216 (1989) 222–248.
[26] R.L. Schwoebel, E.J. Shipsey, Journal of Applied Physics 37 (1966) 3682.
[27] J.A. Blackman, A. Wilding, Europhysics Letters 16 (1991) 115–120.
[28] J.G. Amar, F. Family, P.-M. Lam, Physical Review B (Condensed Matter) 50 (1994) 8781–8797.
[29] P. Meakin, Physical Review A (General Physics) 27 (1983) 1495–1507.
[30] T.A. Witten Jr., L.M. Sander, Physical Review Letters 47 (1981) 1400–1403.
[31] H. Kiessig, Annals of Physics 5 (1931) 769.